Organic Light-Emitting Diodes Based on Silandiol-Bay-Bridged Perylene Bisimides

Felix Brust, Oliver Nagler, Kazutaka Shoyama, Matthias Stolte,* and Frank Würthner*

Perylene bisimides (PBIs) are among the best fluorophores but have to be enwrapped for optoelectronic applications by large and heavy substituents to prevent their $\pi-\pi$-stacking, which is known to accelerate non-radiative decay processes in the solid state. Here, light-weight di-*tert*-butylsilyl groups are introduced to bridge 1,12-dihydroxy and 1,6,7,12-tetrahydroxy PBIs to afford sublimable dyes for vacuum-processed optoelectronic devices. For both new compounds, this substitution provides a twisted and shielded perylene π-core whose, via O—Si—O—bridges, rigid structure affords well-resolved absorption and emission spectra with strong fluorescence in solution, as well as in the solid state. The usefulness of these dyes for vacuum-processed optoelectronic devices is demonstrated in organic light-emitting diodes (OLEDs) that show monomer-like emission spectra and high maximum external quantum efficiency (EQE_{max}) values of up to 3.1% for the doubly silicon-bridged PBI.

1. Introduction

For the fast-growing field of organic electronics, motivated by the ambition of developing earth-abundant environmentally friendly, less toxic, and easier processable semiconductor materials, perylene bisimide (PBI) dyes have gained tremendous attention over the last decades.[1–4] Being already applied as commercial high-performance color pigments and fluorescent dyes, these colorful molecules are especially suited for real-world applications due to their exceptional thermal and chemical stability, high electron-affinity, as well as their outstanding photochemical properties, like fluorescence quantum yields (Φ_{fl}) up to unity.[5–7] Taking this into account, PBIs are perfect

candidates, for example, fluorescence biolabeling,[8,9] luminescent solar concentrators,[10,11] or light emitting devices like solid-state lasers, microcavity photonic devices, and organic light-emitting diodes (OLEDs).[12–17] For all of those applications as emitter materials it is, however, important to prevent the intimate $\pi-\pi$-stacking of PBIs, which results in low-emissive H-aggregates.[18] These intermolecular interactions between PBI dyes are most pronounced in their respective solid state where they enable a large variety of non-radiative relaxation pathways like excimer formation or symmetry-breaking charge separation, resulting in the quenching of fluorescence or additional red-shifted bands, thereby reducing the color purity.[19,20]

To address this issue, different approaches for the suppression of such intermolecular interactions in matrices or the pristine solid-state were developed.[21] Those strategies so far all comprise sterical shielding of the PBI's π-core by large substitutions with bulky groups in either ortho-, imide-, or bay-positions. For ortho-substituted PBIs, the groups of Shinokubo and Osuka were the pioneers with a tetra-*n*-hexyl substituted derivative in 2009 reaching a high solid-state fluorescence quantum yield of 59%.[22] For the other positions, following earlier work of BASF and Langhals,[23–25] our group and the group of Sastre–Santos introduced bulky phenol substituents to the 1,7- bay positions to afford "encapsulated" chromophores[12,26,27] whereas the Wong group applied more bulky imide substituents.[28–31] Both measures proved to be successful by retaining sharp vibronic progressions in solution and thin films along with excellent solid-state fluorescence. In addition, the groups of Sastre–Santos and Wong demonstrated the usefulness of these dyes in solution-processed polymer films for lasing and solar concentrator devices. Besides that, the 1,7- bay substitution was further developed by our group, and recently, even more shielded chromophores with quantum yields above 82% in crystalline solids were obtained.[32,33]

The drawback of this sterical shielding concept is the resulting overall high molecular weight (M_w) with just 20–40% chromophore content of the total mass involving a big amount of non-emitting material, which is needed for effective shielding.[33] Additionally, this increase in M_w renders most of these materials unsuitable for vacuum sublimation, which is desirable for better purification as well as high-performance OLED fabrication. Accordingly, PBI-containing OLEDs fabricated in the last decade mainly relied on fourfold phenoxy

F. Brust, O. Nagler, K. Shoyama, M. Stolte, F. Würthner
Universität Würzburg
Center for Nanosystems Chemistry (CNC)
Theodor-Boveri-Weg
97074 Würzburg, Germany
E-mail: matthias.stolte@uni-wuerzburg.de; wuerthner@uni-wuerzburg.de
K. Shoyama, M. Stolte, F. Würthner
Universität Würzburg
Institut für Organische Chemie
Am Hubland
97074 Würzburg, Germany

The ORCID identification number(s) for the author(s) of this article can be found under https://doi.org/10.1002/adom.202202676.

ADVANCED
SCIENCE NEWS

www.advancedsciencenews.com

ADVANCED
OPTICAL
MATERIALS

www.advopticalmat.de

bay-substituted PBIs,[34] 1,7- direct arylated PBIs,[35] BN-fused PBIs,[16,36] and *N*-annulated PBIs dimers,[15,37] that afforded maximum external quantum efficiency (EQE$_{max}$) values in the range of 0.6–1.6%.
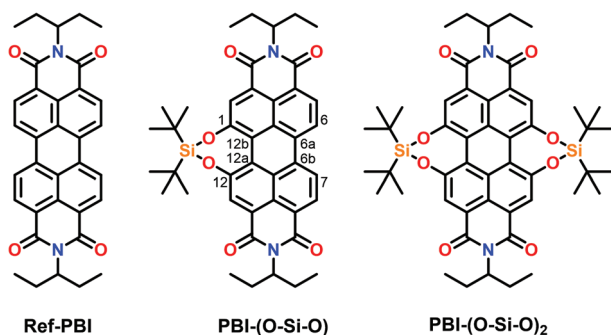
Therefore, with the goal of OLED applications in mind, we designed and synthesized two new light-weight but still well-shielded solid state emitters by introducing *tert*-butylsilyl groups as bay-bridging units to 1,12-dihydroxy- or 1,6,7,12-tetrahydroxy-PBI chromophores. The optical properties of these new non-planar but still rigid compounds were investigated by UV/vis absorption and fluorescence spectroscopy in solution, as a polycrystalline powder or individual microcrystal, as well as embedded in *m*CBP matrix. The successful inhibition of π-contacts in the solid state even for the singly bridged molecule was elucidated by single crystal X-ray structure analysis and correlated to the observed emission spectra and high quantum yields. The utilization of these light-weight dyes as an active component in vacuum-processed devices provided narrow photoluminescence spectra exhibiting devices with EQEs which are among the best for PBI-containing OLEDs.

## 2. Results and Discussion

2.1. Synthesis and X-Ray Analysis

The syntheses of the two new silicon bay-bridged chromophores **PBI−(O−Si−O)** and **PBI−(O−Si−O)₂** are closely related to our just recently reported procedure for carbon-bridged derivatives.[38] The precursors are 1,12-dihydroxy and 1,6,7,12-tetrahydroxy PBI with a small 3-pentyl imide substituent obtained from either 1,12-dihydroxylated perylene bisanhydride or 1,6,7,12-tetra methoxylated PBIs, respectively.[38–40] The hydroxylated molecules **PBI−(OH)₂** and **PBI−(OH)₄** were reacted with appropriate equivalents of di-*tert*-butylsilyl-bis(trifluormethanesulfonate) (DTBS-Ditriflate) at room temperature in the presence of triethylamine as a base to obtain singly bay-bridged compound **PBI−(O−Si−O)** in a high yield of 82%, as well as the doubly bay-bridged **PBI−(O−Si−O)₂** in an almost quantitative yield of 99% (**Scheme 1**, for details, see Supporting Information).

The bridging of bay-oxygen atoms by one or two DTBS groups induces a pronounced twist of the chromophores' π-surface and thereby imparts these dyes with excellent solubility in common organic solvents. Using a small imide substituent, the molecular weight is kept quite low ($M_w = 702.92$ g mol⁻¹ for **PBI−(O−Si−O)** and $M_w = 875.22$ g mol⁻¹ for **PBI−(O−Si−O)₂**) compared to previously reported solid state emitting PBIs with molecular weights of at least 1000 g mol⁻¹ but for most examples, $M_w > 1400$ g mol⁻¹.[29,33] Nevertheless, the chromophore core is still well shielded to prevent π-stacking, which can be deduced from the packing arrangement found in single crystal structures. Single crystals suitable for X-ray analysis were grown for the two new compounds **PBI−(O−Si−O)** and **PBI−(O−Si−O)₂** (**Figure 1**) after the addition of methanol to a saturated dichloromethane solution and subsequent slow crystallization. For **PBI−(O−Si−O)**, the space group is *Pca2₁* whereas **PBI−(O−Si−O)₂** crystalizes in the *P2₁/c* space group (Table S1 and Figures S1–S4, Supporting Information). Both crystal structures comprise *M*- and *P*-enantiomers of the heavily twisted chromophores. The single crystal of **PBI−(O−Si−O)** includes two different conformers that exhibit dihedral angles for the unsubstituted sides of 1° and 7.9° (∢ (C$_6$−C$_{6a}$−C$_{6b}$−C$_7$)), as well as 25° and 24.3° for the bay-bridged sides (∢ (C$_1$−C$_{12b}$−C$_{12a}$−C$_{12}$)), respectively. For the doubly bridged **PBI−(O−Si−O)₂** angles of 24.2° and 26.1° are induced by the strained seven-membered rings (Figure 1a).
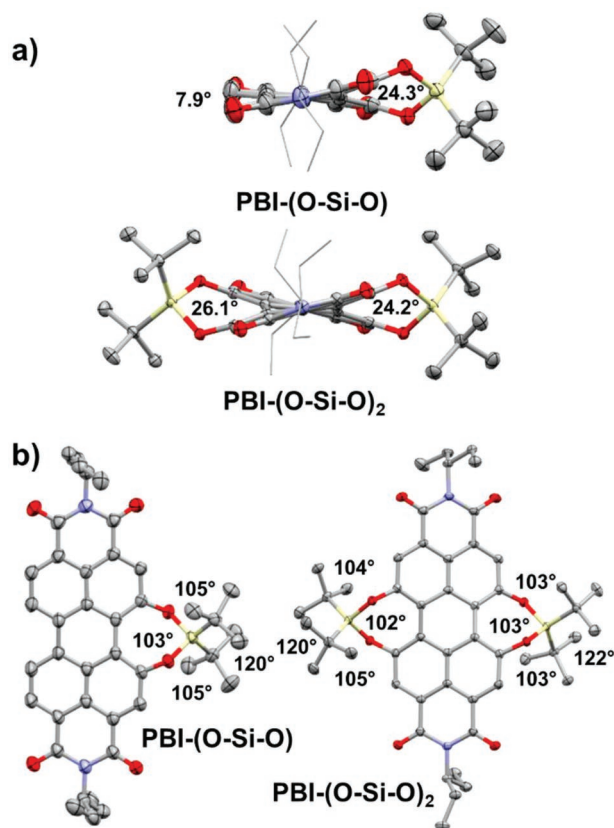
Figure 1. Solid-state molecular structures of **PBI−(O−Si−O)** and **PBI−(O−Si−O)₂** as determined by single-crystal X-ray structure analysis: a) View along the *N,N´* axis with twist angles of each bay-region of the perylene core and b) top view onto the π-surface with relevant bond angles. Ellipsoids are set to 50% probability. Hydrogen atoms, disorder, and solvent molecules are omitted for clarity.


Scheme 1. Singly and doubly silicon bay-bridged perylene bisimides **PBI−(O−Si−O)** and **PBI−(O−Si−O)₂** and **Ref-PBI** included in this study for comparison.

2202676 (2 of 8)

These values suggest little strain energy imparted by the O—Si—O bridging because similar values were previously reported for at bay position with oxygen atoms functionalized PBIs, for example, tetramethoxy substituted PBIs show dihedral angles between 26° and 30°[40,41] and 1,12-dihydroxy substituted PBIs featuring *intra*molecular and *inter*molecular hydrogen bonds are characterized by a dihedral angle of 26.2°.[38] Nevertheless, no stable *M*- or *P*- enantiomers can be separated at room temperature, which differs from tetra-arylated PBIs with stable enantiomers.[42]

As for the dihedral angles of the PBI core discussed above, also the O—Si—O angles of the seven-membered ring appear fairly ideal and not causing significant strain energy. Indeed, for the singly and doubly bridged PBIs O—Si—O angles of 103° are observed that are slightly smaller compared to those of literature-known related BINOL derivatives bearing the same DTBS-group (106°). Further, the lengths of the Si—O bonds in this ring are 1.65 Å, which is in good agreement with the one found for the related BINOL derivatives.[43]

2.2. Optical Properties

The optical properties of the new bay-bridged **PBI—(O—Si—O)** and **PBI—(O—Si—O)₂** were investigated by UV/vis absorption and fluorescence spectroscopy in chloroform solution, and furthermore, in the solid state as powder, as individual microcrystals and embedded in a solid matrix of 3,3′-di(9*H*-carbazol-9-yl)-1,1′-biphenyl (*m*CBP, 15 nm) with 1 wt% PBI. The introduction of the bulky and rigidifying DBTS bridging unit(s) at the chromophore cores does not significantly alter the shape of the vibronic absorption and emission spectra with respect to the spectra of the planar, unsubstituted **Ref-PBI** with the same 3-pentyl imide substituent. Just a bathochromic shift of about 17 (600 cm⁻¹) and 20 nm (700 cm⁻¹) is observable for absorption (λ_{Abs}) and emission (λ_{Em}) maxima, respectively. Similar to related carbon-bridged derivatives,[38] the silicon bay-bridged PBIs also show spectra with a well-resolved vibronic progression for their S_0–S_1 transition in solution, although the chromophore backbone is heavily twisted (Figure 1). Interestingly, **PBI—(O—Si—O)** and **PBI—(O—Si—O)₂** display almost identical absorption spectra with both their λ_{Abs} at 543 nm and molar extinction coefficients (ε_{max}) of 66 000 and 64 000 M⁻¹ cm⁻¹, respectively, which are by about 21% reduced compared to that of **Ref-PBI**. The less-intense S_0–S_2 transition shows a small bathochromic shift to longer wavelengths from 404 to 426 nm for the doubly bridged PBI while the molar extinction coefficients are equal with around 9000 M⁻¹ cm⁻¹. Both compounds display strong yellow emission at 553 nm with marginal Stokes shifts ($\Delta\tilde{\nu}_{Stokes}$) of 350–400 cm⁻¹ and high fluorescence quantum yields (Φ_{fl}) of 89% and 96% for **PBI—(O—Si—O)** and **PBI—(O—Si—O)₂**, respectively (**Figure 2** and **Table 1**).

As desired, polycrystalline powders of **PBI—(O—Si—O)** and **PBI—(O—Si—O)₂** exhibit still vibronically well-resolved emission spectra with solid-state fluorescence quantum yields reaching values of 33% and 42%, respectively (Figure 2a,b), after correction for reabsorption (for details see Figure S5, Supporting Information).[44] This appreciable high Φ_{fl} can
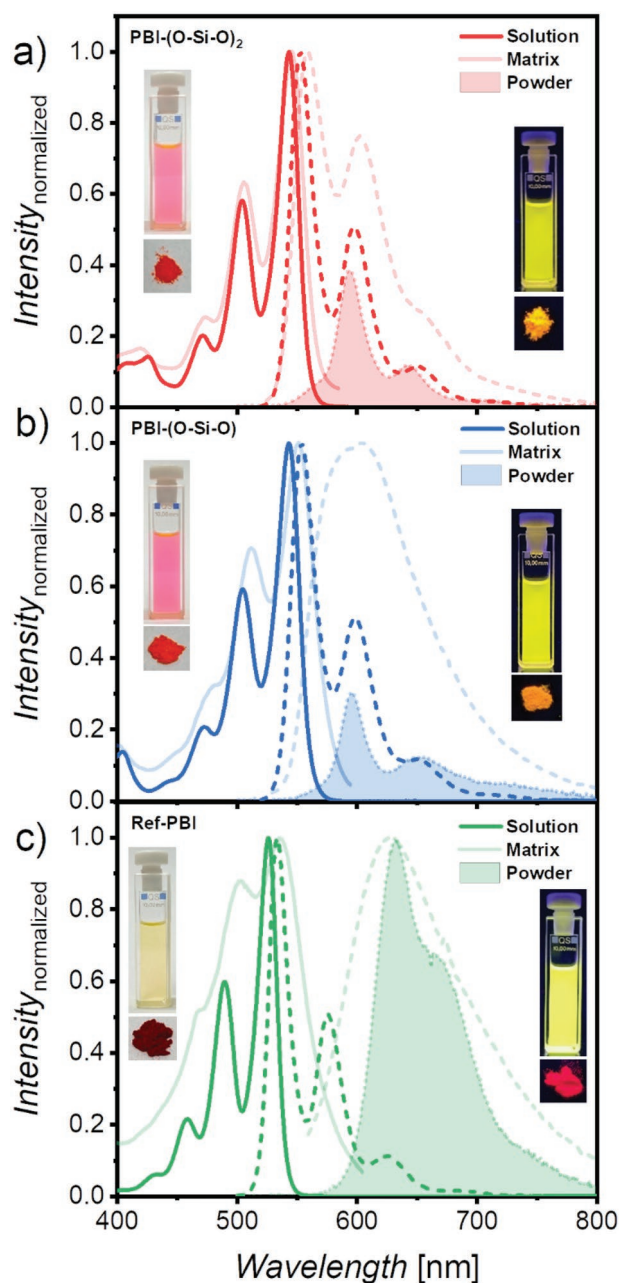
Figure 2. Optical spectra of a) **PBI—(O—Si—O)₂** (red), b) **PBI—(O—Si—O)** (blue), and c) **Ref-PBI** (green). Normalized UV/vis absorption ($c = 20$ μM and $c = 10$ μM for **Ref-PBI**, chloroform, dark color) and excitation spectra at 1 wt% in *m*CBP matrix (light color) displayed as solid lines each with respective normalized emission spectra (dashed lines) and powder spectra (dotted/filled area) scaled according to their reabsorption-free red-edged emission band and normalized for **Ref-PBI**. Insets: Photographs of chloroform solution and powder of compounds under visible light (left) and UV light (right).

readily compete with the best-reported values for PBI-based solid-state emitters—especially at such low M_w (Figure S6, Supporting Information). These findings can be rationalized by their respective molecular packing in the unit cells which display no π–π-stacking, which is normally responsible for the quenching of fluorescence in the solid state. The

Table 1. Optical properties of **PBI−(O−Si−O)**, **PBI−(O−Si−O)₂**, and **Ref-PBI** in solution (CHCl₃), in *m*CBP matrix (1 wt%), and as solid powders at room temperature.

PBI		λ_{Abs} (ε_{max}) [nm (10^3 M^{-1} cm^{-1})]	$A_{00}A_{01}^{-1}$ [1]	λ_{Em} [nm]	$\Delta\tilde{\nu}_{Stokes}$ [cm^{-1}]	Φ_{fl} [%]	τ_{fl}[d] [ns]
PBI−(O−Si−O)₂	Solution (CHCl₃)	543 (64)	1.72	553	350	96[b]	5.11[e]
	Matrix 1 wt%	546[a]	1.58	559	450	–	–
	Powder	–	–	594	–	34 (42)[c]	–
PBI−(O−Si−O)	Solution (CHCl₃)	543 (66)	1.69	554	400	89[b]	4.71[e]
	Matrix 1 wt%	552[a]	1.42	603	1550	–	–
	Powder	–	–	597	–	28 (33)[c]	–
ef-PBI	Solution (CHCl₃)	526 (84)	1.67	533	250	98[b]	3.88[e]
	Matrix 1 wt%	537[a]	0.72	629	2700	–	–
	Powder	–	–	633	–	33[c]	–

[a]Value from the excitation spectra of PBIs in *m*CBP matrix (1 wt%); [b]Relative fluorescence quantum yield determined by the optical dilution method with *N,N'*-bis(2,6-diisopropylphenyl)-1,6,7,12-tetraphenoxyperylene-3,4:9,10-bis(dicarboximide) (Φ_{fl} = 96% in chloroform) or *N,N'*-bis(2,6-diisopropylphenyl)-perylene-3,4:9,10-bis(dicarboximide) (Φ_{fl} = 100% in chloroform) as the references; [c]Absolute quantum yield measured (quantum yield corrected for reabsorption)[44]; [d]Fluorescence lifetime measured with EPL-510 picosecond pulsed diode laser (λ_{ex} = 505.8 nm); [e]Value with a standard deviation of about 7×10^{-12} s.

chromophore center-to-center distance for **PBI−(O−Si−O)** is 8.7 Å while **PBI−(O−Si−O)₂** displays two different values with 7.4 and 8.3 Å to its next neighbor molecules, representing therewith indeed quite isolated perylene cores. Furthermore, rather pronounced longitudinal and transversal slips are observed in the respective packing arrangements for both **PBI−(O−Si−O)** and **PBI−(O−Si−O)₂** (Figures S2 and S3, Supporting Information), thereby leading to negligible Coulomb couplings.[45]

Interestingly, the two compounds doped in the *m*CBP matrix (1 wt%) exhibit very different optical properties. The doubly bay-bridged best-shielded **PBI−(O−Si−O)₂** still shows well-resolved excitation (546 nm) and emission (559 nm) spectra that are only slightly bathochromically-shifted compared to the spectra of monomers in solution with an A_{00}/A_{01} ratio from 1.72 (solution) down to 1.58 in *m*CBP matrix. In contrast, **PBI−(O−Si−O)** in *m*CBP matrix exhibits a slightly broadened excitation spectrum (552 nm) with a decreased A_{00}/A_{01} ratio from 1.69 (solution) down to 1.42, as well as a significantly red-shifted and broad excimer-like emission (603 nm), similar to dimer or extended stacks of co-facially aggregated PBIs (Figure 2a,b).[46] Thus, the excitation and emission spectra resemble more those of the planar, non-shielded **Ref-PBI** with its equally broad and structureless emission spectrum. This is attributable to π-stacked chromophores which are prevalent even at such low doping ratios and whose structures may resemble those found for **Ref-PBI** or in its crystal structure.[47,48] Here, the maximum is even further red-shifted to 629 nm (Table 1) and the A_{00}/A_{01} ratio in solution with 1.67 is decreased to 1.14, indicating H-aggregation (Figure 2c). With an A_{00}/A_{01} ratio of 0.72 in the neat thin film, the aggregation is even more pronounced (Figure S7, Supporting Information).
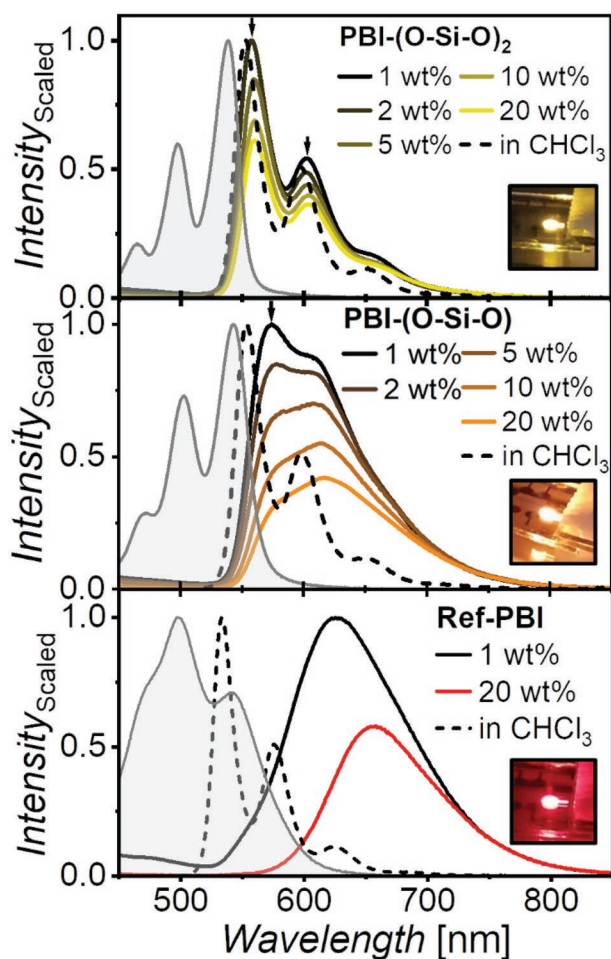
Comparing the two emission spectra of **PBI−(O−Si−O)** as polycrystalline powders with the ones in *m*CBP matrix (1 wt%), two completely different shapes can be observed. The broad and structureless emission along with the reduced A_{00}/A_{01} ratio of the excitation spectrum in *m*CBP indicates the formation of PBI H-aggregates in the matrix even at such low doping ratios.

2.3. OLED Devices

2.3.1. Device Fabrication

To investigate the performance of these solid-state emitters as active materials in OLEDs, devices with the following layer structure were produced all by sublimation in a vacuum: ITO/MoO₃/TBBD/TCTA/**PBI** in *m*CBP/PPF/TPBi/Liq/Al (for details see Supporting Information). The device structure follows a standard structure of OLEDs, starting with MoO₃ as the hole injection layer, TBBD as the hole transport layer, and TCTA as the electron blocking layer. To obtain the 30 nm thick active layer, each PBI derivative was evaporated simultaneously with the host material *m*CBP. Their deposition rates are controlled by quartz microbalances to ensure that the desired emitter ratio in the active layer ranging from 1, 2, 5, 10, up to 20 wt% is achieved. Interestingly, despite the higher molecular weight, the two bay-bridged PBIs **PBI−(O−Si−O)** and **PBI−(O−Si−O)₂** afford a stable sublimation rate already at 205 °C ($p < 5 \times 10^{-6}$ mbar) while for **Ref-PBI** a 15 °C higher temperature was needed. This demonstrates the impact of π−π-stacking interactions for these dyes on the cohesive energy as can be also seen by their respective enthalpies of melting in our differential scanning calorimetry studies (for details see Figure S10, Supporting Information). To explore the impact of the Si-bridging on the device performance, additional OLEDs were processed employing an unsubstituted **Ref-PBI** with identical imide substituent for the lowest and highest concentrations (1 and 20 wt%). Evaporated on top of the active layer were in order: PPF as the hole-blocking layer, TPBi as the electron transport layer, Liq as an injection layer, and finally, Aluminum, as a metallic top contact. A small investigation regarding the positive effects of the blocking layers can be found in the Supporting Information (Figure S8, Supporting Information).

**ADVANCED
SCIENCE NEWS**

www.advancedsciencenews.com

**ADVANCED
OPTICAL
MATERIALS**

www.advopticalmat.de

Figure 3. Electroluminescence spectra of OLEDs based on **PBI−(O−Si−O)₂** (top, yellow), **PBI−(O−Si−O)** (middle, orange), and **Ref-PBI** (bottom, red) all recorded at drive voltages of 12 V. The fluorescence spectra measured in CHCl₃ (dashed lines) are displayed for easy comparison. The gray shaded area represents the normalized UV/vis absorption spectra of neat vacuum-deposited thin films on quartz substrates. Displayed in the insets are photographs of operating devices with an active area diameter of 7.1 mm².

2.3.2. Device Electroluminescence

The electroluminescence (EL) spectra displayed in **Figure 3** were recorded driving 1 wt% OLEDs at 12 V bias and are scaled to the reabsorption-free red-edge of each emission spectrum. All three materials show distinct spectral shapes, and accordingly, the color of their EL. The most shielded chromophore **PBI−(O−Si−O)₂** displays like in the previous optical studies a clean monomer-like emission spectrum with EL maximum (λ_{EL}) at 558 nm along with a well-resolved vibronic progression similar to what could be observed in solution (Figure 2). These findings corroborate that the chromophores are successfully rigidified by the Si-bridge, as well as sufficiently isolated by the DBTS groups, resulting in the well-defined emission structure, also in mCBP matrix.[38] The yellow device emission corresponds to CIE xy coordinates of (0.48, 0.49).

PBI−(O−Si−O) exhibits broader EL spectra reaching up to 750 nm with a prominent λ_{EL} at 580 nm (1 wt%) that shifts

with rising emitter concentration to higher wavelengths up to 617 nm (20 wt%). This is probably caused by self-absorption of the active layer as the flank of the absorption spectrum of the material extends out to 600 nm. Interestingly, these device EL spectra are seemingly less defined than both solution and solid state PL spectra in Figure 2, where **PBI−(O−Si−O)** shows clear monomer-like emission. In the device matrix, however, it seems that at low concentrations, some emitter molecules already started to aggregate, supported by the reduced A_{00}/A_{01} ratio compared to **PBI−(O−Si−O)₂**.[49] The increase in the A_{01} band intensity hints at a partial formation of H-aggregates in mCBP matrix. This is, surprisingly, in conflict with the crystal structures (Figures S2 and S3, Supporting Information), where all chromophores apparently are oriented equidistant to each other and do not show any kind of π-stacking. In contrast to the yellow emission of **PBI−(O−Si−O)₂**, the devices of single bay-bridged **PBI−(O−Si−O)** emit orange light at (0.54, 0.43).

Ref-PBI shows already at low concentration (1 wt%) a broad and structureless red emission at 627 nm with CIE coordinates of (0.57, 0.36). With increasing doping ratio λ_{EL} shifts further bathochromically due to self-absorption at higher emitter concentrations. The broad featureless emission spectrum combined with the dominant A_{01} absorption band are clear indications that the observed electroluminescence of **Ref-PBI** is attributable to H-aggregates in the solid matrix of the OLED devices.[48]

2.3.3. Device Performance

In order to assess the effectiveness of both novel materials as OLED emitters, two series of devices with the layer structure shown in **Figure 4**a and varying weight ratios of each PBI emitter material in mCBP matrices were fabricated. In Figure 4b, the EQEs of all manufactured devices at a luminance of 100 cd m⁻² are shown. For the weight ratio of 1 wt%, both J–V–L- and EQE-curves are shown in Figure 4c,d and their characteristics parameters are listed in **Table 2**.

As has previously been reported for PBI-based OLEDs, we also see a decrease in efficiency with a rising concentration of emitter molecules in the devices.[36] The stronger drop-off in efficiency for higher emitter amounts for the doubly bridged **PBI−(O−Si−O)₂** might be related to the differences in the solid-state molecular packing to **PBI−(O−Si−O)**.

All three materials show similar turn-on voltage at around 5 V. However, both Si-bay-bridged PBIs show a clear improvement in efficiency over the reference material **Ref-PBI**, considering both the 1 and 20 wt% devices. The EQE at a luminance of 100 cd m⁻² (EQE₁₀₀) of **PBI−(O−Si−O)₂** of 1.9% is almost twice that of the **Ref-PBI** (1.1%) with **PBI−(O−Si−O)** also showing an improved output with 1.4%. Furthermore, devices employing **PBI−(O−Si−O)₂** average a maximum EQE of 3.1%, comparing very well to other values reported in the literatures for PBI-containing OLEDs.[15,35,36] The **PBI−(O−Si−O)₂** OLEDs also exhibit 50% higher luminescence at high driving voltages than devices using **PBI−(O−Si−O)** or **Ref-PBI**. Additionally, noteworthy is that the current efficiency at a luminance of 100 cd m⁻² ($\mu_{L,100}$) improves by 120% from the **Ref-PBI** ($\mu_{L,100}$ = 0.7 cd A⁻¹) to **PBI−(O−Si−O)** with 1.6 cd A⁻¹.
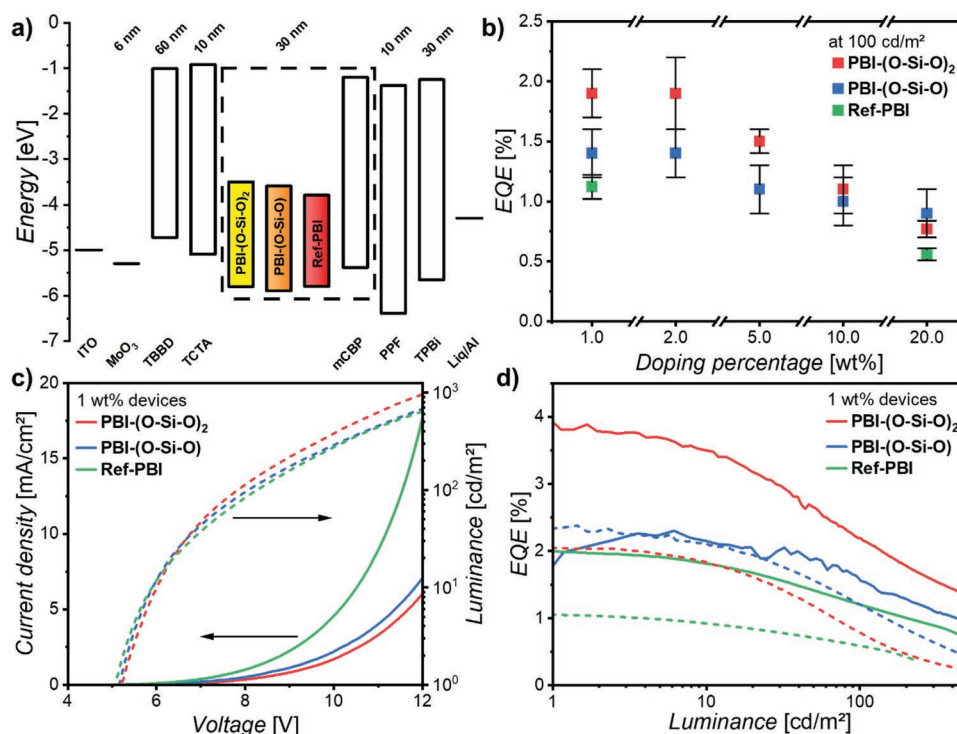
Figure 4. a) Device architecture used for all OLED devices with the electronic energy levels of employed materials. b) PBI doping percentage-dependent device efficiency at 100 cd m^{-2} of OLEDs of **PBI−(O−Si−O)** (blue), **PBI−(O−Si−O)$_2$** (red), and **Ref-PBI** (green) in *m*CBP matrix. c) *J–V–L* and d) EQE/*L* curves for the 1 wt% devices. The dashed lines in (d) represent the EQE curves of devices with 20 wt% PBI emitters as a comparison.

The doubly bridged **PBI−(O−Si−O)$_2$** shows an even bigger enhancement of over 250% with a current efficiency of up to 2.6 cd A^{-1}. A further advantage of the additional steric shielding by the Silicon-bay bridging is the consistency of the emission spectrum of **PBI−(O−Si−O)$_2$** regardless of doping percentage. While **PBI−(O−Si−O)** and **Ref-PBI** exhibit small changes in color with rising amounts of dopant in the active layer, **PBI−(O−Si−O)$_2$** shows almost no color change, likely thanks to the very effective shielding of the chromophore (Figure S9, Supporting Information).

It can thus be concluded that next to the higher thermal stability, the silicon bay-bridging also has a positive effect on the performance of PBIs used as OLED singlet emitters. Especially at very low dopant amounts in *m*CBP, where only limited interactions between the emitter molecules should be possible, the bridged PBIs show a remarkable increase in efficiency. This suggests that the improvement is not only due to improved π-shielding caused by the steric demand DTBS units added to the bay position of the chromophore core. These results show that **PBI−(O−Si−O)$_2$** is the best emitter molecule of the three

showing higher efficiencies and reaching higher luminances than both the **Ref-PBI** and the singly bridged **PBI−(O−Si−O)**.

3. Conclusion

Two new PBI derivatives bearing one or two bulky di-*tert*-butyl-silyl-groups at their bay areas were synthesized. These two dyes with almost identical narrow absorption and emission properties show very high fluorescence quantum yields close to unity in solution. In their solid state, these values are well retained with up to 42% and can easily compete with the best candidates for PBI-based solid state emitters while still keeping the molecular weight low. The high fluorescence in the solid is maintained due to the efficient shielding of the chromophore π-cores in the respective crystal structures. With these advantageous properties along with the optical features, both molecules have been successfully implemented as emitter material into vacuum-processed OLEDs using *m*CBP as the matrix. For PBI-based OLED devices with an EQE of up to 1.9% at a luminance

Table 2. OLEDs device properties based on emitting layers of *m*CBP with 1 wt% of derivatives **PBI−(O−Si−O)$_2$**, **PBI−(O−Si−O)**, and **Ref-PBI**.

1 wt% of	EQE$_{max}$ [%]	EQE$_{100}$[a] [%]	V_{TO}[b] [V]	$\lambda_{EL,max}$ [nm]	$\mu_{L,100}$[a] [cd A^{-1}]	L_{12V} [cd m^{-2}]	T_{sub}[d] [°C]
PBI−(O−Si−O)$_2$	3.1 ± 0.9	1.9 ± 0.2	5.3 ± 0.2	560	2.6 ± 0.3	1000 ± 100	205
PBI−(O−Si−O)	2.0 ± 0.4	1.4 ± 0.2	5.22 ± 0.06	575	1.6 ± 0.2	590 ± 50	205
Ref-PBI	1.5 ± 0.4	1.1 ± 0.1	5.04 ± 0.03	626	0.7 ± 0.1	640 ± 30	220

[a]Evaluated at *L* = 100 cd m^{-2}; [b]Evaluated at *L* = 1 cd m^{-2}; [c]Evaluated at V = 12 V; [d]Sublimation temperature required to produce 1 wt% active layers with *m*CBP with a rate of 0.5 Å s^{-1} at 10^{-7} mbar. Number of investigated devices: **PBI−(O−Si−O)$_2$**: 28, **PBI−(O−Si−O)**: 12, **Ref-PBI**: 17.

**ADVANCED
SCIENCE NEWS**

www.advancedsciencenews.com

**ADVANCED
OPTICAL
MATERIALS**

www.advopticalmat.de

of 100 cd m^{-2} and electroluminescence emission maxima at 560 nm for **PBI−(O−Si−O)$_2$** with monomeric spectral shape, our devices are among the best-performing ones for this class of dyes reported to date.

4. Experimental Section

Experimental procedures, sample preparation, and characterization details can be found in Supporting Information.

CCDC 2216669 and 2216670 contain supplementary crystallographic data for this paper. These data can be obtained free of charge from The Cambridge Crystallographic Data Centre via www.ccdc.cam.ac.uk/data_request/cif.

Supporting Information

Supporting Information is available from the Wiley Online Library or from the author.

Conflict of Interest

The authors declare no conflict of interest.

Data Availability Statement

The data that support the findings of this study are available from the corresponding author upon reasonable request.

[1] X. Zhan, A. Facchetti, S. Barlow, T. J. Marks, M. A. Ratner, M. R. Wasielewski, S. R. Marder, *Adv. Mater.* **2011**, *23*, 268.

[2] S. Chen, P. Slattum, C. Wang, L. Zang, *Chem. Rev.* **2015**, *115*, 11967.

[3] M. Sun, K. Müllen, M. Yin, *Chem. Soc. Rev.* **2016**, *45*, 1513.

[4] A. Nowak-Król, F. Würthner, *Org. Chem. Front.* **2019**, *6*, 1272.

[5] F. C. De Schryver, T. Vosch, M. Cotlet, M. Van der Auweraer, K. Müllen, J. Hofkens, *Acc. Chem. Res.* **2005**, *38*, 514.

[6] A. Herrmann, K. Müllen, *Chem. Lett.* **2006**, *35*, 978.

[7] F. Würthner, C. R. Saha-Möller, B. Fimmel, S. Ogi, P. Leowanawat, D. Schmidt, *Chem. Rev.* **2016**, *116*, 962.

[8] S. K. Yang, X. Shi, S. Park, S. Doganay, T. Ha, S. C. Zimmermann, *J. Am. Chem. Soc.* **2011**, *133*, 9964.

[9] Z. Xu, W. Cheng, K. Guo, J. Yu, J. Shen, J. Tang, W. Yang, M. Yin, *ACS Appl. Mater. Interfaces* **2015**, *7*, 9784.

[10] B. McKenna, R. C. Evans, *Adv. Mater.* **2017**, *29*, 1606491.

[11] J. A. H. P. Sol, V. Dehm, R. Hecht, F. Würthner, A. P. H. J. Schenning, M. G. Debije, *Angew. Chem., Int. Ed.* **2018**, *57*, 1030; *Angew. Chem.* **2018**, *130*, 1042.

[12] M. G. Ramírez, S. Pla, P. G. Boj, J. M. Villavilla, J. A. Quintana, M. A. Díaz-García, F. Fernández-Lázaro, Á. Sastre-Santos, *Adv. Opt. Mater.* **2013**, *1*, 933.

[13] A. J. C. Kuehne, M. C. Gather, *Chem. Rev.* **2016**, *116*, 12823.

[14] P. Lova, V. Grande, G. Manfredi, M. Patrini, S. Herbst, F. Würthner, D. Comoretto, *Adv. Opt. Mater.* **2017**, *5*, 1700523.

[15] S. V. Dayneko, E. Cieplechowicz, S. S. Bhojgude, J. F. Van Humbeck, M. Pahlevani, G. C. Welch, *Mater. Adv.* **2021**, *2*, 933.

[16] J. Hoffmann, B. Geffroy, E. Jaques, M. Hissler, A. Staubitz, *J. Mater. Chem. C* **2021**, *9*, 14720.

[17] S. Izawa, M. Morimoto, S. Naka, M. Hiramoto, *Adv. Opt. Mater.* **2022**, *10*, 2101710.

[18] J. Sung, P. Kim, B. Fimmel, F. Würthner, D. Kim, *Nat. Commun.* **2015**, *6*, 8646.

[19] C. Kaufmann, W. Kim, A. Nowak-Król, Y. Hong, D. Kim, F. Würthner, *J. Am. Chem. Soc.* **2018**, *140*, 4253.

[20] G. Ran, J. Zeb, Y. Song, P. A. Denis, U. Ghani, W. Zhang, *J. Phys. Chem. C* **2022**, *126*, 3872.

[21] J. Gierschner, J. Shi, B. Milián-Medina, D. Roca-Sanjuán, S. Varghese, S. Park, *Adv. Opt. Mater.* **2021**, *9*, 2002251.

[22] S. Nakazono, Y. Imazaki, H. Yoo, J. Yang, T. Sasamori, N. Tokitoh, T. Cédric, H. Kageyama, D. Kim, H. Shinokubo, A. Osuka, *Chem. - Eur. J.* **2009**, *15*, 7530.

[23] G. Seybold, G. Wagenblast, *Dyes Pigm.* **1989**, *11*, 303.

[24] R. Reisfeld, G. Seybold, *Chimia* **1990**, *44*, 295.

[25] H. Langhals, O. Krotz, K. Polborn, P. Mayer, *Angew. Chem., Int. Ed.* **2005**, *44*, 2427.

[26] M.-J. Lin, Á. Jiménez, C. Burschka, F. Würthner, *Chem. Commun.* **2012**, *48*, 12050.

[27] Á. Jiménez, M.-J. Lin, C. Burschka, J. Becker, V. Settels, B. Engels, F. Würthner, *Chem. Sci.* **2014**, *5*, 608.

[28] J. L. Banal, H. Soleimaninejad, F. M. Jradi, M. Liu, J. M. White, A. W. Blakers, M. W. Cooper, D. J. Jones, K. P. Ghiggino, S. R. Marder, T. A. Smith, W. W. H. Wong, *J. Phys. Chem. C* **2016**, *120*, 12952.

[29] B. Zhang, H. Soleimaninejad, D. J. Jones, J. M. White, K. P. Ghiggino, T. A. Smith, W. W. H. Wong, *Chem. Mater.* **2017**, *29*, 8395.

[30] B. Zhang, P. Zhao, L. J. Wilson, J. Subbiah, H. Yang, P. Mulvaney, D. J. Jones, K. P. Ghiggino, W. W. H. Wong, *ACS Energy Lett.* **2019**, *4*, 1839.

[31] R. P. Sabatini, B. Zhang, A. Gupta, J. Leoni, W. W. H. Wong, G. Lakhwani, *J. Mater. Chem. C* **2019**, *7*, 2954.

[32] D. Schmidt, M. Stolte, J. Süß, A. Liess, V. Stepanenko, F. Würthner, *Angew. Chem., Int. Ed.* **2019**, *58*, 13385; *Angew. Chem.* **2019**, *131*, 13519.

[33] M. Stolte, T. Schembri, J. Süß, D. Schmidt, A.-M. Krause, M. O. Vysotsky, F. Würthner, *Chem. Mater.* **2020**, *32*, 6222.

[34] F. J. Céspedes-Guirao, S. García-Santamaría, F. Fernández-Lázaro, Á. Sastre-Santos, H. J. Bolink, *J. Phys. D: Appl. Phys.* **2009**, *42*, 105106.

[35] E. Kozma, W. Mróz, F. Villafiorita-Monteleone, F. Galeotti, A. Andicsová-Eckstein, M. Catellani, C. Botta, *RSC Adv.* **2016**, *6*, 61175.

**ADVANCED
SCIENCE NEWS**

www.advancedsciencenews.com

**ADVANCED
OPTICAL
MATERIALS**

www.advopticalmat.de

[36] G. Li, Y. Zhao, J. Li, J. Cao, J. Zhu, X. W. Sun, Q. Zhang, *J. Org. Chem.* **2015**, *80*, 196.

[37] S. V. Dayneko, M. Rahmati, M. Pahlevani, G. C. Welch, *J. Mater. Chem. C* **2020**, *8*, 2314.

[38] O. Nagler, A.-M. Krause, K. Shoyama, M. Stolte, R. K. Dubey, L. Liu, Z. Xie, F. Würthner, *Org. Lett.* **2022**, *24*, 6839.

[39] P. Leowanawat, A. Nowak-Król, F. Würthner, *Org. Chem. Front.* **2016**, *3*, 537.

[40] X. Wen, A. Nowak-Król, O. Nagler, F. Kraus, N. Zhu, N. Zheng, M. Müller, D. Schmidt, Z. Xie, F. Würthner, *Angew. Chem.* **2019**, *131*, 13185; *Angew. Chem., Int. Ed.* **2019**, *58*, 13051.

[41] A. Nowak-Król, M. I. S. Röhr, D. Schmidt, F. Würthner, *Angew. Chem.* **2017**, *129*, 11936; *Angew. Chem., Int. Ed.* **2017**, *56*, 11774.

[42] R. Renner, M. Stolte, J. Heitmüller, T. Brixner, C. Lambert, F. Würthner, *Mater. Horiz.* **2022**, *9*, 350.

[43] J. F. Schneider, M. Nieger, K. Nättinen, B. Lewall, E. Niecke, K. H. Dötz, *Eur. J. Org. Chem.* **2005**, *2005*, 1541.

[44] T.-S. Ahn, R. O. Al-Kaysi, A. M. Müller, K. M. Wentz, C. J. Bardeen, *Rev. Sci. Instrum.* **2007**, *78*, 086105.

[45] D. Bialas, E. Kirchner, M. I. S. Röhr, F. Würthner, *J. Am. Chem. Soc.* **2021**, *143*, 4500.

[46] M. Son, K. H. Park, C. Shao, F. Würthner, D. Kim, *J. Phys. Chem. Lett.* **2014**, *5*, 3601.

[47] X. Zhang, B. Sun, *J. Phys. Chem. B* **2007**, *111*, 10881.

[48] W. Maniukiewicz, J. Bojarska, A. Olczak, E. Dobruchowska, M. Wiatrowski, *Acta Crystallogr., Sect. E: Crystallogr. Commun.* **2010**, *66*, o2570.

[49] F. C. Spano, *Acc. Chem. Res.* **2010**, *43*, 429.